

Pyrometamorphic rocks associated with naturally burned coal beds, Powder River Basin, Wyoming*

MICHAEL A. COSCA, ERIC J. ESSENE

Department of Geological Sciences, University of Michigan, Ann Arbor, Michigan 48109, U.S.A.

JOHN W. GEISSMAN

Department of Geology, University of New Mexico, Albuquerque, New Mexico 87131, U.S.A.

WILLIAM B. SIMMONS

Department of Earth Sciences, University of New Orleans, New Orleans, Louisiana 70148, U.S.A.

DONALD A. COATES

U.S. Geological Survey, Denver Federal Center, Denver, Colorado 80225, U.S.A.

ABSTRACT

Glass-bearing pyrometamorphic melt-rock, formed during natural burning of Tertiary coal in the Powder River Basin, Wyoming, contains a variety of high-temperature igneous minerals, some with diverse and unusual compositions. The melt-rock or *paralava*, was transformed from coal-ash and overlying Tertiary sedimentary rocks through local heating to fusion temperatures. Paralava bulk compositions differ from overlying and surrounding baked sedimentary rocks, or *clinker*, by marked depletions of Si, Al, and K and enrichments in Fe, Mg, and Ca. Paralava contains a variety of phenocryst and quench minerals including fayalitic olivine, tridymite, cristobalite, sekaninaite (Fe end-member cordierite), anorthite, magnetite-hercynite-ulvöspinel solid solutions, hematite-ilmenite solid solutions, pseudobrookite, melilite solid solutions, aluminous clinopyroxenes, a rhönite-like phase (dorrite), titanian andradite, wollastonite, mullite, enstatite, potassium and barium feldspars, apatite, sahamalite, and nepheline. Glass compositions have been used to estimate minimum temperatures of paralava formation and are in the range 1020 to 1400 °C. It is suggested that varying degrees of disequilibrium melting, mixing, crystallization, volatilization, and liquid immiscibility are involved during paralava formation. Although rare in nature, the minerals and textures observed in paralava have affinities to more common igneous rocks and may provide insight into other high-temperature processes in geologic systems.

INTRODUCTION

Pyrometamorphism occurs at ultra-high temperatures (>1000 °C) and low pressures (≤ 1 kbar) and often results in fusion of near-surface sediments. The Mottled Zone of Israel (Matthews and Gross, 1980) and the buchites in Scotland (Tilley, 1924) are well-known examples where many high-temperature minerals were first identified. Pyrometamorphism is probably most well known from reports of dry basaltic intrusions and their effects on included xenoliths of surrounding, usually sedimentary, country rocks (e.g., Tilley, 1924; Agrell and Langley, 1958; Wyllie, 1961; Smith, 1969; Grapes, 1986). Less well known but equally widespread are pyrometamorphic (combustion metamorphic) rocks associated with bituminous sedimentary rocks (McLintock, 1932; Bentor and Kastner, 1976; Bentor et al., 1981; Bentor, 1984) and

combusted coal beds (e.g., Fermor, 1918; Baker, 1953; Whitworth, 1958; Church et al., 1979).

Although many areas contain pyrometamorphic rocks formed through natural coal combustion, few quantitative data have been obtained on these rocks, and less information is available regarding their physical conditions of formation. Some data are available for rocks produced by natural combustion of bituminous sedimentary rocks of the Monterey Formation (Bentor et al., 1981). Based on variations in major- and trace-element compositions, Bentor et al. (1981) made distinctions between low-temperature melts (LTM), and higher-temperature melts (HTM). Although not well constrained, formation temperatures were estimated at 1000 °C (LTM) to 1650 °C (HTM). As discussed in this paper, some similarities exist between the combustion metamorphic rocks derived from bituminous sedimentary rocks of the Monterey Formation (Bentor et al., 1981) and those formed by natural coal combustion, but the detailed mineral and whole-rock compositional data are distinct.

* Contribution no. 450 from the Mineralogical Laboratory, Department of Geological Sciences, University of Michigan.

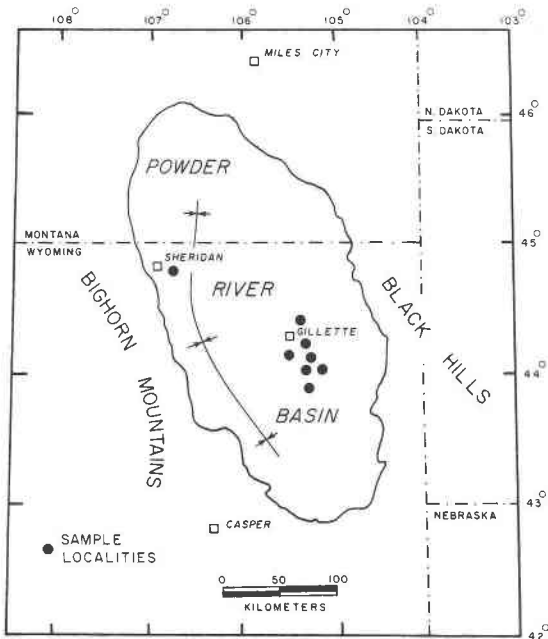


Fig. 1. Sample location map showing outline of the Powder River Basin.

Mineral formation associated with coal combustion is dependent on many physical and chemical variables including the original sediment bulk composition, temperature, degree of melting, and oxidation state. The degree to which one or more of these factors affects mineral stabilities may be variable on the scale of a thin section. However, certain field and petrographic observations combined with analytical data may constrain the relative importance of the various possible controls. The purpose of this study is to report mineral and whole-rock compositional data for pyrometamorphic rocks associated with combusted coal beds of the Powder River Basin, Wyoming (Fig. 1), and to provide some constraints on their formation conditions. The samples collected for this study have been roughly separated into rocks that were thermally altered but unmelted, termed *clinker*, and those that were fused, termed *paralava* (Fermor, 1918; Venkatesh, 1952). Although the term *clinker* is accepted in the geological literature to include all rocks altered by coal combustion, separation of rock types is important to avoid ambiguities and therefore the additional term *paralava* is used for the purposes of this paper. Samples of clinker and paralava were collected from outcrops in the PRB near Gillette, Wyoming (Fig. 1). They were examined petrographically, by electron-microprobe analysis (EMPA), X-ray fluorescence (XRF), and X-ray diffraction (XRD) techniques.

REGIONAL GEOLOGY

The Powder River Basin is an elongate basin covering approximately 37000 km² between the Bighorn Mountains and the Black Hills and extends north into southern

Montana (Fig. 1). Cretaceous and Tertiary sedimentary rocks on the east side of the basin dip gently toward its axis in response to late Laramide orogenic activity (West, 1964). Exposed through erosion and ignited by natural processes, near-surface burning of Tertiary coal in the basin has produced large volumes of thermally altered sedimentary rocks (Bastin, 1905; Rogers, 1918; May, 1954; Sigsby, 1966; Bauer, 1972; Jackson, 1981; Budai and Cummings, 1984; Coates and Naeser, 1984; Essene et al., 1984; Cosca and Essene, 1985; Foit et al., 1987).

Coal fires were probably first initiated when coal was exposed to the atmosphere through erosion and was either spontaneously combusted or ignited by lightning or prairie fires (Rogers, 1918). Indeed, spontaneous combustion of coal is a common phenomenon (Raask, 1985) and is often observed in many of the open-pit coal mines within the Powder River Basin. Alternatively, C- and O-isotope data from vegetation growing around a vent produced by present-day burning of coal in Canada indicate that ground water is involved as an oxidant (Gleason and Kyser, 1984). Regardless of the cause in the Powder River Basin, once ignited, a burning "front" advances below the surface following the coal bed, periodically vents, and operates as a natural blast furnace as long as adequate fuel and oxygen are available. Consequently, much of the basin's current landscape is in the form of mesas and buttes capped by erosion-resistant, bright red to orange clinker. From a distance, many of the outcrops exhibit sharply contrasting light-colored sedimentary rocks below the bright capping of clinker. Fission-track dates from detrital zircons contained in northeastern Powder River Basin clinker indicate that the burn zones become progressively older to the east, ranging in age from 0.08 to 0.77 ± 0.39 Ma (Coates and Naeser, 1984). Paleomagnetic reversal data reveal that some clinkers in the northern part of the basin formed more than 1.4 Ma ago (Jones et al., 1984). Ignition of coal in other basins has resulted in a semicontinuous belt of clinker-bearing sediments stretching from Texas to Canada (Rogers, 1918; Bentor, 1984).

Paralava and clinker of the Powder River Basin were derived from continental sedimentary rocks of the Fort Union and Wasatch Formations. The Fort Union Formation is Paleocene in age and is a thick sequence (600–900 m) of interbedded sandstones, shales, siltstones, limestones, and coal beds (Glass, 1976). The uppermost 250 m of the Fort Union Formation is dominated by fine-grained sandstone, siltstone, shale, and coal. Coal beds within this formation are a major economic resource with some in this area exceeding thicknesses of 25 m (Denson and Keefer, 1974). Conformably overlying the Fort Union Formation is the Eocene Wasatch Formation (Glass, 1976). The Wasatch Formation (300–700 m) crops out over much of the central part of the basin and contains numerous siltstones, fine-grained sandstones, coals, and some thin beds of ferruginous nodules. Coal beds within the Wasatch Formation are concentrated in the lower portion and are generally 1–5 m thick, but they locally may attain thicknesses of 70 m (Glass, 1976).

OCCURRENCE OF PYROMETAMORPHIC ROCK

The degree of thermal alteration produced by burning coal beds is variable, and a single outcrop (sometimes exceeding thicknesses of 30 m) may contain altered rock ranging from slightly baked (clinker) to entirely fused (paralava). In close proximity to a heat source (gas vent or burnt coal bed), clinker becomes streaked and porcelaneous, and it may become partly or completely fused to form paralava. Typical examples of paralava outcrop include the following: (1) layers or lenses, presumed to represent original sedimentary horizons; (2) small, commonly spherical globules that may represent incipient melting; and (3) vesicular, chimneylike pipes or dikes of paralava often containing clasts of unfused clinker.

The observed rock types and features associated with a combusted coal bed are schematically illustrated in Figure 2. Below the coal ash, the rocks consist of a thick sequence of unaltered, well-sorted siltstones and sandstones, sandy conglomerates, and occasional layers of feruginous nodules. In many instances, a sharp contact is observed separating underlying unaltered sedimentary rocks from thermally metamorphosed equivalents; the contact has been interpreted to be recording a paleo-water table (Baker, 1953; Budai and Cummings, 1984). If so, a well-defined record of paleo-water tables, temporally constrained by fission-track or paleomagnetic methods, may prove useful for reconstructing paleohydrologic environments. Alternatively, this contact may simply represent a boundary across which little heat is transferred (Bustin and Mathews, 1982), implying that the majority of heat was dissipated either laterally or upward by advection, with only a small component of heat transferred downward by conduction.

A regular, gradational pattern of partially to completely combusted coal, coal-ash, paralava, and baked, nonmelted clinker occurs above the unaltered sedimentary rocks (Fig. 2). The residual coal layer, if present, is generally a few centimeters to two meters thick and grades from black to gray to white upward in section; it has been referred to as coke (Bustin and Mathews, 1982; Merrit, 1985). The coke grades upward into a distinctive white ash layer, approximately 15–25 cm thick, containing thin layers of banded and porcelaneous shale near the upper contact of the coal bed. Where observed, the contact at the top of the ash zone is sharp and underlies a 15–20 cm thick, highly vesicular, light brown to green paralava with abundant glass. The glass-rich paralava may have been derived from fusion of residual coal ash and/or immediately overlying sediment and indicates that intense heating occurred within, or centimeters above, the coal beds. The paralava grades upward into a thick, laterally continuous sequence of baked and reddened clinker. Clinker occurs in a variety of colors including various shades of yellow, green, red, purple, black, gray, and bleached white. Relict bedding is generally preserved, although local heating and melting may obscure or totally obliterate original structures.

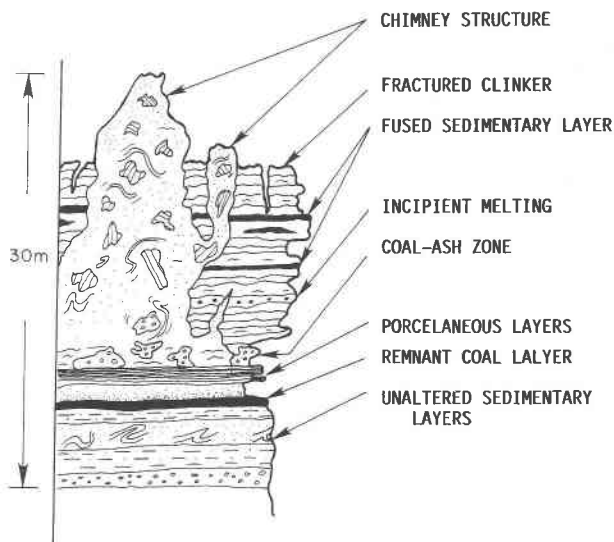


Fig. 2. Schematic cross-section through a typical clinker- and paralava-bearing outcrop in the Powder River Basin. The chimney structure is composed of black and vesiculated paralava containing clasts of clinkers. The coal-ash zone contains glassy, vesicular paralava.

Erosion-resistant chimney structures (pipes) are present to some extent in nearly every clinker outcrop and may reach 5–15 m in height. The chimneys usually contain angular clasts of clinker up to 0.5 m in diameter within a massive matrix of black, vesicular paralava. Many slump and drip textures contained in the paralava and flow structures developed around clinker clasts resemble pahoehoe lava and indicate relatively low viscosities. Paralava similar to that in the chimneys is developed in subvertical fractures within clinker that probably acted as conduits for hot gases or channels along which paralava was either formed or flowed. Breccias are locally developed in many chimneys, possibly reflecting violent combustion events. Similar chimneys have been observed in paralava outcrops in Australia (Baker, 1953), southern Utah (W. P. Nash, pers. comm.), and also from the combustion metamorphic rocks of the Monterey Formation (Bentor et al., 1981). The chimneys have been interpreted to develop by gravitational collapse into the cavities left by the combusted coal bed (Baker, 1953). The black paralava contained in the chimneys is the most abundant type of paralava observed in outcrops of the Powder River Basin. Its abundance, phenocryst minerals, and flow textures suggest that this paralava has formed almost entirely from a liquid. Similar conclusions were reached by Bentor et al. (1981) for the massive HTM rocks of the Monterey Formation.

ANALYTICAL METHODS

EMPA

Quantative mineral and glass analyses were performed using a Cameca CAMEBAX microprobe. For most crystalline phases, a 15-kV accelerating potential, 10-nA sample current, and a fo-

TABLE 1. Representative mineral compositions from Powder River Basin paralava

Sample: Phase:	L-14 Sp	83E-38A Sp	AM-7 Sp	DR-7 Mel	DR-7 Pg	DR-8 Cpx	C-3 Cpx	C-30 Mul	83EU-2 Ol
SiO ₂	n.d.	0.13	n.d.	29.84	43.17	30.32	37.63	29.72	30.96
TiO ₂	1.61	10.98	n.d.	0.13	n.d.	1.10	3.46	0.42	n.d.
Al ₂ O ₃	40.04	10.87	19.20	23.23	35.84	18.95	18.23	61.48	0.40
Fe ₂ O ₃ *	20.09	33.91	57.84	3.60	1.08	21.69	7.40	7.28	n.d.
Cr ₂ O ₃	0.21	0.69	n.d.	n.d.	n.d.	n.d.	n.d.	n.d.	n.d.
FeO*	37.24	42.81	1.78	1.23	n.d.	0.48	0.46	n.d.	64.26
MnO	0.24	0.13	0.46	0.05	0.01	0.08	0.03	n.d.	0.66
MgO	0.94	0.17	20.93	3.11	n.d.	2.97	8.83	0.57	3.94
ZnO	n.d.	0.06	n.d.	n.d.	n.d.	n.d.	n.d.	n.d.	n.d.
CaO	n.d.	n.d.	n.d.	38.24	19.72	23.75	24.28	n.d.	0.04
Na ₂ O	n.d.	n.d.	n.d.	1.19	0.08	0.14	0.16	0.03	n.d.
K ₂ O	n.d.	n.d.	n.d.	n.d.	0.03	n.d.	n.d.	n.d.	n.d.
Total	100.37	99.75	100.21	100.62	99.93	99.48	100.48	99.50	100.26
Si	0.0	0.005	0.0	1.372	2.007	1.208	1.404	1.636	1.013
Ti	0.038	0.297	0.0	0.005	0.0	0.033	0.097	0.017	0.0
Al	1.468	0.460	0.684	1.259	1.964	0.890	0.812	3.989	0.015
Fe ³⁺ *	0.470	0.917	1.316	0.113	0.038	0.650	0.208	0.302	0.0
Cr	0.005	0.020	0.0	0.0	0.0	0.0	0.0	0.0	0.0
Fe ²⁺ *	0.969	1.287	0.045	0.043	0.0	0.016	0.013	0.0	1.759
Mn	0.006	0.004	0.012	0.002	0.0	0.003	0.001	0.0	0.018
Mg	0.044	0.009	0.943	0.213	0.0	0.176	0.491	0.047	0.192
Zn	0.0	0.002	0.0	0.0	0.0	0.0	0.0	0.0	0.0
Ca	0.0	0.0	0.0	1.884	0.983	1.014	0.972	0.0	0.001
Na	0.0	0.0	0.0	0.106	0.008	0.011	0.012	0.003	0.0
K	0.0	0.0	0.0	0.0	0.001	0.0	0.0	0.0	0.0
Sample: Phase:	83EM-5 Opx	DR-8 Dr	C-35 Ne	C-11 Mel	KM-5 Hem	83E-27 Psbr	83E-38A Ol	DR-8 Wo	L-8 Bfs
SiO ₂	56.54	11.34	44.85	43.34	0.04	0.10	31.07	50.55	39.82
TiO ₂	0.12	0.59	n.d.	0.04	0.23	21.45	0.0	0.30	0.38
Al ₂ O ₃	2.07	25.71	34.95	10.90	1.35	5.78	0.39	0.24	27.33
Fe ₂ O ₃ *	n.d.	39.27	1.18	1.24	97.32	71.24	n.d.	n.d.	1.13
Cr ₂ O ₃	n.d.	0.10	n.d.	n.d.	n.d.	0.36	n.d.	n.d.	n.d.
FeO*	9.82	2.91	n.d.	n.d.	n.d.	n.d.	63.75	0.43	n.d.
MnO	n.d.	0.22	n.d.	n.d.	0.82	0.24	0.57	0.27	0.02
MgO	31.21	5.50	0.04	7.07	0.18	0.35	4.39	n.d.	0.06
BaO	n.d.	n.d.	n.d.	n.d.	n.d.	n.d.	n.d.	n.d.	26.73
CaO	0.88	13.66	3.65	32.69	n.d.	n.d.	0.01	47.68	2.12
Na ₂ O	n.d.	0.05	12.20	4.21	n.d.	n.d.	n.d.	0.06	1.45
K ₂ O	0.09	0.01	3.65	0.04	n.d.	n.d.	n.d.	0.08	0.83
Total	100.73	99.36	100.52	99.53	99.94	99.52	100.18	99.61	99.85
Si	0.984	1.632	1.031	1.921	0.001	0.003	1.015	0.982	2.216
Ti	0.002	0.064	0.0	0.001	0.004	0.623	0.0	0.004	0.016
Al	0.042	4.361	0.947	0.569	0.042	0.263	0.015	0.005	1.792
Fe ³⁺ *	0.0	4.250	0.021	0.042	1.928	2.069	0.0	0.0	0.047
Cr	0.0	0.013	0.0	0.0	0.0	0.110	0.0	0.0	0.0
Fe ²⁺ *	0.143	0.350	0.0	0.0	0.0	0.0	1.741	0.007	0.0
Mn	0.0	0.026	0.0	0.0	0.018	0.008	0.015	0.004	0.013
Mg	0.809	1.179	0.001	0.467	0.007	0.020	0.0	0.0	0.052
Ba	0.0	0.0	0.0	0.0	0.0	0.0	0.0	0.0	0.583
Ca	0.016	2.107	0.090	1.553	0.0	0.0	0.0	0.993	0.126
Na	0.0	0.013	0.544	0.361	0.0	0.0	0.0	0.002	0.156
K	0.002	0.0	0.107	0.002	0.0	0.0	0.0	0.002	0.059

Note: Sp: spinel solid solutions; Mel: melilite; Pg: plagioclase; Cp: clinopyroxene; Mul: mullite; Ol: olivine; Opx: orthopyroxene; Dr: dorrite; Ne: nepheline; Hem: hematite; Psbr: pseudobrookite; Bfs: Ba-feldspar. Atomic fractions calculated on the basis of cations; n.d. = not determined.

* Calculated from normalized formula.

cused electron beam were standard operating conditions. Alkali volatilization from the glasses necessitated a different set of operating conditions. Conditions were optimized with a focused electron beam rastered over a 1.5- μm^2 area with an accelerating potential of 12 kV and sample current of 5–10 nA; alkali volatilization was minimal under these conditions. Well-characterized natural and synthetic standards were used and were periodically checked during analytical sessions and corrected for any instrumental drift.

XRF

The xrf analyses were conducted individually by two of us in separate laboratories at New Orleans (W.B.S.) and at Michigan (M.A.C.). Because of the unusual compositions of these rocks, some xrf analyses were problematic in that the unknowns (paralava) have a distinct and unusual composition compared to the ordinary rock standards. Hence, the large mass absorption corrections yield erratic totals. Major-element analyses at New Orleans performed by the pressed pellet method gave widely vari-

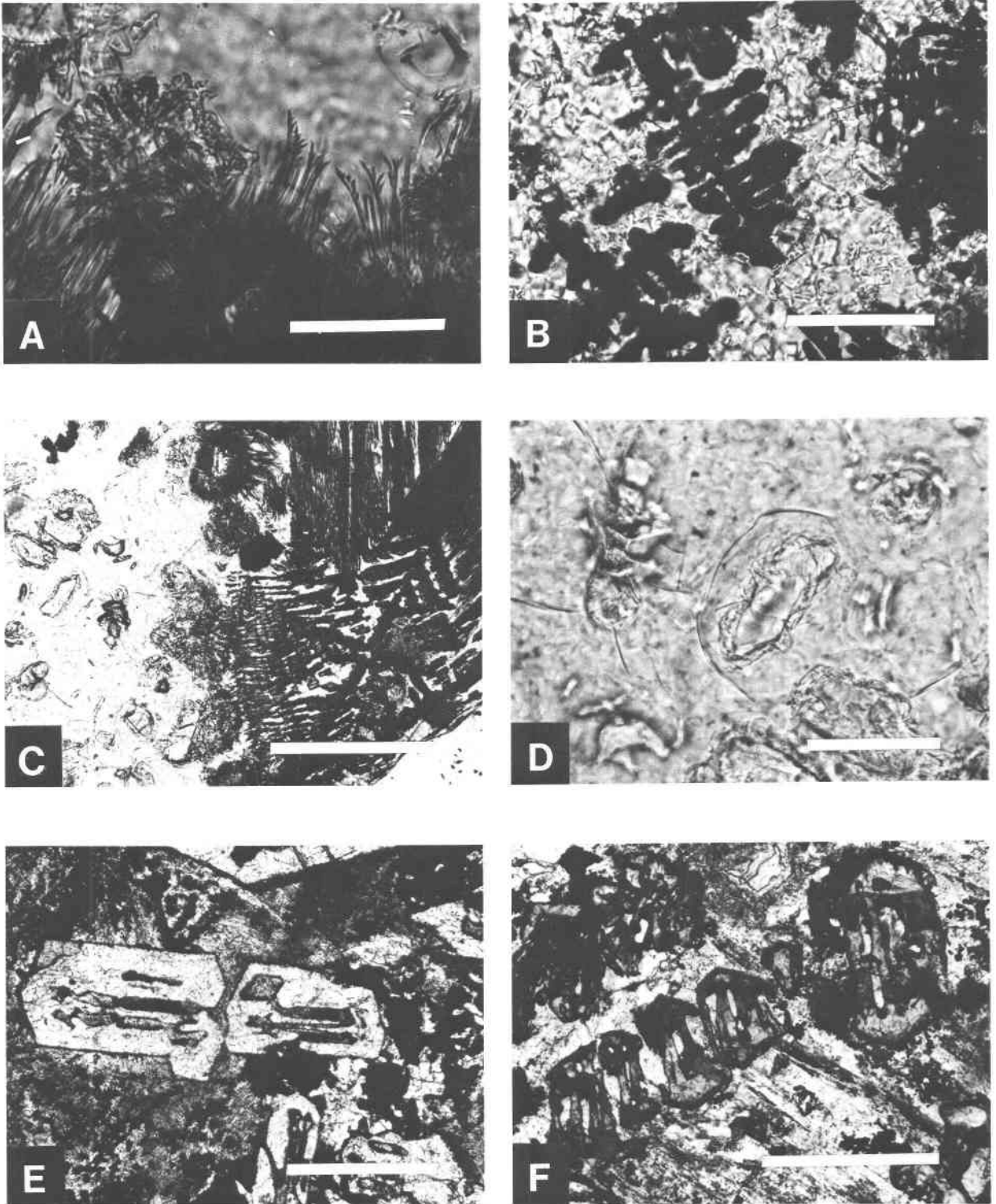


Fig. 3. Quenched mineral textures occurring in paralava. (A) Glass containing feathery clinopyroxene and a partially melted detrital quartz grain (upper right) (scale bar = 25 μm). (B) Skeletal framework of hematite contained in a glass matrix (scale bar = 50 μm). (C) Symmetrically branching, quenched framework of clinopyroxene within a glass matrix. Note partially fused detrital quartz grains (scale bar = 200 μm). (D) Enlargement of a detrital quartz grain from C exhibiting a glass rind gradational into the matrix glass (scale bar = 50 μm). (E) and (F) Skeletal crystals of olivine associated with glass and spinel solid solutions (scale bar = 250 μm). All photographs taken in plane-polarized light.

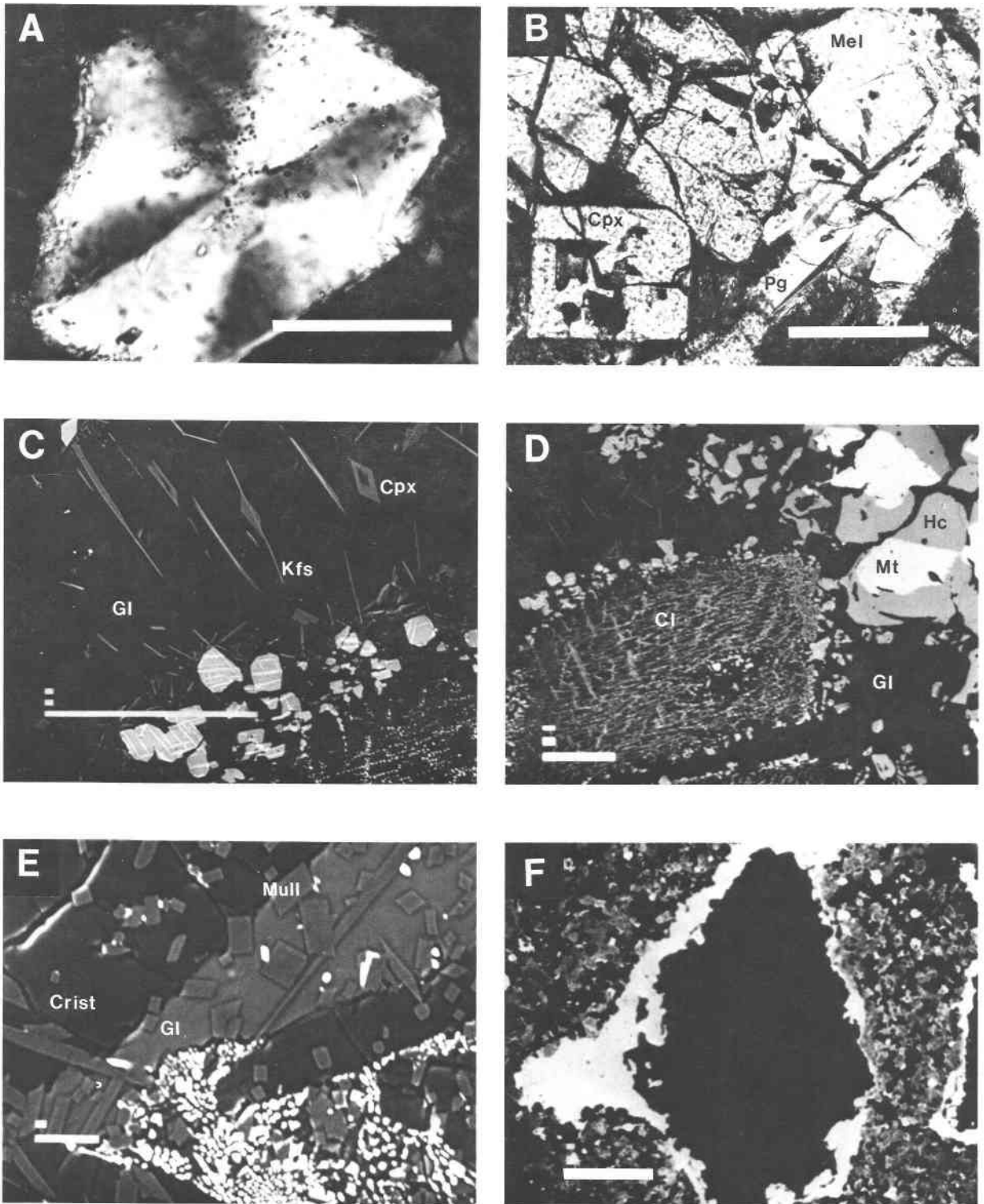


Fig. 4. (A) Cyclic twinning in cordierite (photograph taken under crossed polars with accessory plate) (scale bar = 100 μm). (B) Plane-polarized-light photograph of coexisting clinopyroxene (Cpx), melilite (Mel), and plagioclase (Pg) (scale bar = 500 μm). (C) Backscattered-electron (BSE) photograph of paralava glass (Gl) (see enlargement in C). Also shown are two-phase mixtures of magnetite and hercynite solid solutions (scale bar = 100 μm)

and potassium feldspar (Kfs). Note the boxwork exsolution of magnetite from a hercynite host (scale bar = 100 μm). (D) BSE photograph of a fused clinker fragment (Cl) forming fine-grained oxides and silicates within a matrix of crystallite-bearing glass (Gl) (see enlargement in C). Also shown are two-phase mixtures of magnetite and hercynite solid solutions (scale bar = 100 μm).

able results, probably the result of strong mineral effects. Samples and additional standards prepared as fused disks were employed at Michigan and yielded somewhat better precision through analytical totals (excluding LOI) occasionally fell outside the range 98–102%. The occasionally significant –LOI is primarily derived from calcite that is a common vug-filling mineral. The +LOI is obtained from oxidation of the iron oxides during the firing process.

XRD

The X-ray diffraction data were collected on a Phillips powder X-ray diffractometer. Most samples were prepared as powders; however, some hand-picked mineral grains were also analyzed as single grains or agglomerates by Gandolfi techniques for positive identification.

MINERALS IN POWDER RIVER BASIN PARALAVA

A variety of crystalline phases and textures are encountered in paralava. In general, minerals within paralava are coarse enough ($>2 \mu\text{m}$) to quantitatively analyze by EMPA, and representative analyses are presented in Table 1. Minerals from many paralava samples were analyzed both petrographically and chemically, and XRD was used to distinguish different polymorphs. Some phases, especially those occurring as acicular needles, were too small for quantitative analysis, and a combination of petrographic, XRD, and qualitative EDS techniques was used for mineral identification. In addition to the larger detrital grains, unmelted clinker is composed of fine-grained ($<1 \mu\text{m}$) metamorphic minerals (Clark and Peacor, 1987) that require scanning transmission electron-microscope (STEM) analysis for proper characterization.

Abundant features from paralava such as spinifex and hopper crystals, radial mineral clusters surrounded by glass, and crystals aligned around vesicles (Fig. 3) are convincing evidence that these minerals crystallized (quenched) directly from a liquid. In some instances, textural and chemical relationships at the thin-section scale provide strong evidence for local mixing of two or more separate liquids (Cosca et al., 1988). Rapid cooling in paralava may have been produced by the sudden opening of fractures or slumping of overburden, allowing the infiltration of cooler air. Although factors such as the number of nuclei, viscosity, temperature, oxygen fugacity, superliquidus heating, and bulk composition may have some affect on cooling rates, these textures are qualitatively consistent with those produced experimentally in basalts cooled at rates of approximately $30 \text{ }^\circ\text{C/h}$ (Lofgren et al., 1974). Other textures consisting of coarser-grained phenocrysts, similar to many volcanic rocks, are suggestive of somewhat slower cooling from a liquid (Fig. 4B).

Phenocrysts and/or quench crystals identified by opti-

cal petrography, XRD and EMPA/SEM include olivine, enstatite, clinopyroxene, a rhönite-like phase (dorrinite), cristobalite, tridymite, mullite, anorthite, nepheline, garnet, potassium feldspar, barium feldspar, gehlenite–akermanite–sodium melilite solid solutions, sekaninaite (Fe end-member cordierite), apatite, spinel–magnetite–hercynite–ulvöspinel, hematite–ilmenite, and pseudobrookite solid solutions, wollastonite, xenotime, sahamalite, and some unidentified Cu- and Fe-bearing sulfides. Low quartz and zircon were observed in some paralava, presumably surviving as detrital phases even at high temperatures. Some of the phases reported here have been identified in paralava from other parts of the Powder River Basin (Bauer, 1972; Jackson, 1981; Hooper and Foit, 1986; Foit et al., 1987) and from paralava occurrences elsewhere (e.g., Baker, 1953; Whitworth, 1958; Bustin and Mathews, 1982; Hooper, 1982). Not surprisingly, a similar collection of minerals (olivine, cordierite, plagioclase, pyroxene, spinel, and glass) has been reported from slag produced as a byproduct of thermally treated oil shale (Phemister, 1942). Mullite and spinel have also been reported from slag occurring on walls of pulverized coal-fired boilers (Raask, 1985). However, very few chemical data have been previously obtained for phases from natural or synthetic slags.

Pyroxene

Clinopyroxene is a very common mineral in paralava. It occurs both as coarse-grained, equant phenocrysts and as feathery or acicular crystals (Fig. 3). The latter textures may have formed as crystals were quenched from a liquid (Figs. 3 and 4). Clinopyroxenes range in composition from diopside to near end-member esseneite, $\text{CaFe}^{3+}\text{AlSiO}_6$ (Table 1), indicating extensive substitution of Fe^{3+} for Mg in the M1 site coupled with $\text{Al} \pm \text{Fe}^{3+}$ substitution for Si in the tetrahedral site (Cosca et al., 1985; Hooper and Foit, 1986; Cosca and Peacor, 1987; Foit et al., 1987). At 1-bar pressure, oxygen fugacities approaching the hematite–magnetite (H-M) buffer are required to stabilize the most Fe^{3+} -rich pyroxenes (Cosca and Peacor, 1987). Orthopyroxene ($X_{\text{Fe}} = 0.13$) is rare, occurring as fine needles in glass. The general lack of orthopyroxene is consistent with a highly oxidizing environment.

Olivine

Olivine (fayalite) occurs as spinifex-like crystals up to 3 cm in length and also as subhedral skeletal grains 10–15 mm across (Figs. 3E, 3F). The spinifex grains exhibit strong pleochroism (X: yellow green; Y: yellow orange; Z: light green) and are fairly uniform in composition ($X_{\text{Mg}} = 0.03\text{--}0.09$). Olivine coexists with cordierite, cristobalite, and magnetite–hercynite–ulvöspinel solid solutions.

←
(E) BSE photograph of paralava glass (Gl) containing crystals of cristobalite (Crist) displaying shrinkage cracks, penetrating crystals of mullite (Mull) and Fe-Ti oxides (bright) (scale bar = 10 μm). (F) Vesicle in paralava lined with hematite (scale bar = 100 μm).

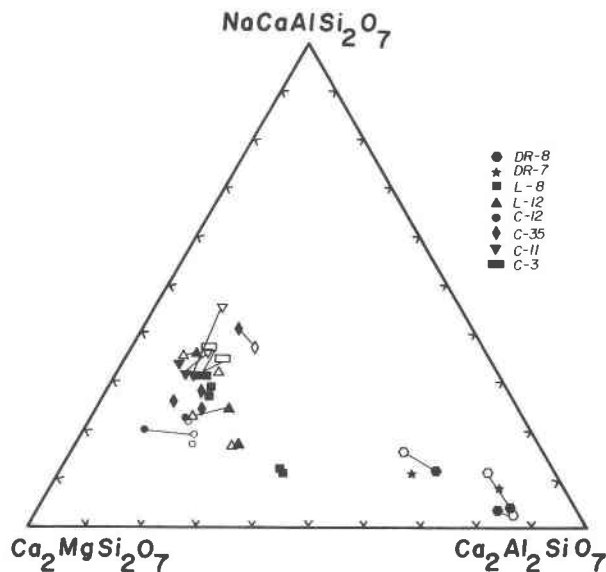


Fig. 5. Compositional projection of melilites from paralava shown within the system $\text{Ca}_2\text{MgSi}_2\text{O}_7$ (akermanite)– $\text{Ca}_2\text{Al}_2\text{SiO}_7$ (gehlenite)– $\text{CaNaAlSi}_2\text{O}_7$ (soda melilite). Symbols correspond to individual point analyses of different samples (solid: core; open: rim).

Many of the olivines contain spinel solid solutions as inclusions.

SiO_2 polymorphs

Paralava may contain any one or all three of the SiO_2 polymorphs quartz, tridymite, and cristobalite. Three SiO_2 polymorphs were observed to coexist in one paralava derived from sandstone, where detrital (low) quartz, tridymite, and cristobalite were identified by XRD. More often only one polymorph is observed, usually cristobalite, occurring as needles in complex interpenetrating textures. Backscattered-electron images illustrate that some cristobalites contain inclusions of mullite and iron oxides and shrinkage cracks formed during cooling that reflect differential thermal contraction (Fig. 4). Quantitative analyses indicate that a small combined percentage (0.1–0.3 wt%) of Al, Fe, and Ti is incorporated into the SiO_2 structure during the transformation of quartz to cristobalite or tridymite, as with tridymite in silica bricks (Schneider and Majdic, 1984, 1985; Seifert-Kraus and Schneider, 1984).

Melilite

Melilite is a common phenocryst in silica-undersaturated paralava occurring as large (10–20 mm) euhedral phenocrysts with aluminous pyroxenes, dorrite, spinel solid solutions, and garnet. Many grains display tetragonal outlines, some are twinned, and many are optically and chemically zoned. Compositions are variable and exist over a wide range of akermanite–gehlenite–sodium melilite solid solutions ($\text{Ak}_{10-70}\text{Geh}_{10-86}\text{SM}_{3-45}$) (Fig. 5). A small amount (2–5%) of ferrigehlenite and ferriakerman-

ite is also present in most samples. No systematic chemical variation is evident in core vs. rim analyses, although many of the rim analyses appear to have a higher concentration of a sodium melilite component (Fig. 5). The large grain size and chemical zoning may imply that the melilite formed under conditions of *relatively* slow cooling. Melilite is readily identified by its low birefringence, uniaxial symmetry, and euhedral shape.

Feldspars

At least three different feldspars have been identified in paralava, but the coarsest and most abundant is anorthite ($\text{An}_{95-97}\text{Ab}_{1-5}\text{Or}_{1-2}$). It occurs as 1–5 mm long, polysynthetically twinned, lath-shaped grains associated with clinopyroxene, dorrite, spinel solid solutions, and, more rarely, with melilite. Some of the anorthite grains are preferentially aligned, indicating they have flowed in a liquid. Other grains appear to have been forcibly displaced around vesicles.

Celsian, hyalophane, and potassium feldspar occur as fine fibers in some paralavas. The Ba feldspars appear restricted to irregular pockets containing radiating crystals in glass formed along grain boundaries. These pockets also contain wollastonite and lesser ulvöspinel and resemble the barred structure of chondrules. Potassium feldspar is present in many samples as 1- to 10- μm -long, acicular crystals usually contained in glass. Their size precludes quantitative analysis, but only K, Al, and Si were observed by EDS.

Dorrite

A newly described rhönite-like mineral called dorrite (ideally $\text{Ca}_2(\text{Mg}_2\text{Fe}_3^{2+})(\text{Al}_4\text{Si}_2)\text{O}_{20}$) with extensive substitutions of both octahedral and tetrahedrally coordinated Fe^{3+} and Al^{3+} occurs in paralava from near the coal–sedimentary rock interface (Cosca et al., 1988). Dorrite is related to rhönite and occurs only in silica-undersaturated paralava usually in the presence of esseneite-rich clinopyroxene, melilite, magnetite, plagioclase, garnet with or without nepheline, apatite, and wollastonite. It is nearly opaque in thin section, and many crystals contain a core of irregularly shaped magnetite, suggesting that the spinel is being replaced by dorrite. The occurrence of dorrite appears restricted to conditions of high temperature and f_{O_2} and may be related to reactions involving pyroxene and magnetite (Cosca et al., 1988).

Cordierite

Cordierite occurs as euhedral grains 2–5 mm in length with hexagonal cross sections. XRD patterns indicate the presence of high cordierite (indialite) and chemical analyses indicate them to be Fe rich ($X_{\text{Fe}} = 0.70$). The cordierite crystals are strongly pleochroic (*O*: violet; *E*: colorless) and many display cyclic twinning (Fig. 4A). Cordierite appears restricted to paralava containing the assemblage fayalite-cristobalite-spinel (magnetite-hercynite), and it is often found in paralavas forming chimney structures.

Oxides

Spinel is widely distributed in paralava. Substitutions involving Fe^{2+} - Fe^{3+} -Al-Ti account for a variety of intermediate spinel-magnetite-hercynite-ulvöspinel compositions. These substitutions are also reflected in solid solutions of hematite-ilmenite and pseudobrookite. Many of the spinels and other oxides have unmixed upon cooling to produce complex intergrowths of magnetite-hercynite-ulvöspinel (Figs. 4C, 4D), hematite, pseudobrookite, and/or ilmenite (Modreski and Herring, 1985). The exsolution patterns indicate subsolvus cooling of a once-homogeneous oxide phase formed at higher temperature. Crystal habits and textures may exhibit extreme variation within a single thin section, from euhedral inclusions to felted or radiating dendritic masses. Many of the oxides are concentrated along small cracks, lining vesicles or other openings that allow access of oxygen and/or metalliferous complexes.

Wollastonite

Wollastonite occurs in accessory quantities as fine needles up to 10 μm long that fluoresce bright blue under the electron beam. Chemical analyses indicate that it is nearly pure (Wo_{99}). It is distinguished from pseudowollastonite by its optical properties (length-slow).

Garnet

Titanian andradite is found in some silica-undersaturated paralavas. It contains up to 6.0 wt% TiO_2 and is associated with melilite, magnetite, clinopyroxene, and dorrite (Cosca et al., 1988). In thin section, garnets are anhedral in shape, yellow-green in color, and commonly display signs of textural disequilibrium.

Apatite

Apatite is an abundant accessory phase typically found as needles included in glass. Qualitative energy-dispersive spectra indicate only the presence of Ca and P.

Mullite

Mullite occurs as prismatic crystals approximately 10–20 μm in length, with cristobalite and glass. Chemical analyses indicate the presence of up to 8 wt% Fe_2O_3 . Mullite is rare in the paralava collected for this study and is probably restricted to the more aluminous sedimentary layers.

Nepheline

Nepheline (carnegieite?) is found in small amounts in some Si-undersaturated paralava and forms the only significant phase concentrating Na in these rocks. Chemical analyses display a small Fe^{3+} content. XRD analysis was not possible because of the small grain size and small number of grains identified. This phase could be carnegieite, a high-temperature polymorph of nepheline.

Sahamalite

Sahamalite $((\text{Mg,Fe})_2(\text{Ce,Nd,Y})_2(\text{CO}_3)_4)$ occurs as metallic, spherical blebs approximately 0–0.5 mm in diameter. It is closely associated with melilite in Si-poor paralava. Qualitative analysis of sahamalite separated from some samples confirmed the presence of Fe, Mg, Ce, Y, and Nd.

Xenotime

Xenotime is occasionally found in paralava as irregularly shaped grains and was identified by EDS from the X-ray peaks of Y and P; no quantitative chemical results were obtained. This phase could be detrital or primary in origin and does not appear restricted to any particular paralava composition.

PARALAVA GLASS COMPOSITIONS

Glass is a common constituent in many paralavas from the Powder River Basin and implies rapid quenching from conditions of high temperature at near-atmospheric pressure. These conditions are geologically rare yet produce a wide range of mineral and chemical diversity. Paralava glasses usually contain a variety of phenocrysts and/or crystals and represent liquid (melt) compositions quenched on or above their liquidus. Because petrographic textures are so similar to those produced artificially, these rocks offer natural analogues to many laboratory experiments conducted at 1 atm.

Brady and Greig (1939) conducted melting experiments with clinker from Arizona and concluded that minimum temperatures of 1117 °C must be reached before melting begins. Similar experiments by Whitworth (1958) required temperatures in excess of 1350 °C before melting was observed. Precise temperatures at which paralavas form may be constrained by examination of glass compositions. Powder River Basin glasses exhibit a limited range in silica content, with somewhat wider variations occurring in Na, K, Ca, Al, and Fe contents (Table 2). If low-pressure phase relations are known, assuming equilibrium melting conditions, a minimum liquidus temperature may be determined for such glasses by comparison with 1-atm experimental data for similar compositions. Glass samples from basin paralavas analyzed by EMPA indicate *minimum* melt temperatures of 1020 to 1400 °C (Table 2). These temperatures were determined by projecting the major components of the glass onto the liquidus of appropriate experimentally determined 1-atm melting diagrams (e.g., Schairer and Bowen, 1947; Schairer, 1950; Osborn and Muan, 1960). Because most ternary melting diagrams are constructed in terms of mineral components on a weight percentage basis (e.g., An-Ab-Or), paralava glass compositions were first computed in terms of their CIPW normative equivalents (in weight percent) and renormalized in terms of the three most abundant components. For most glass compositions, the normative phases are closely approximated by the ternary system $\text{CaAl}_2\text{Si}_2\text{O}_8$ - KAlSi_3O_8 - SiO_2 (Fig. 6). A

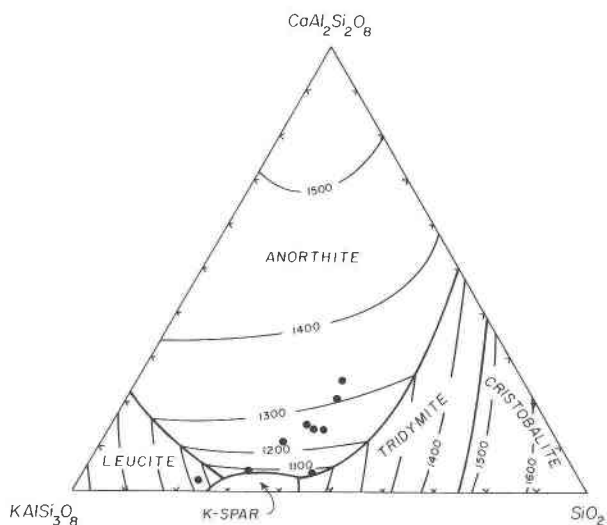


Fig. 6. Normative compositions of paralava glass (filled circles) projected onto the liquidus of the system $\text{CaAl}_2\text{Si}_2\text{O}_8$ - KAlSi_3O_8 - SiO_2 (redrawn from Schairer and Bowen, 1947).

few of the glasses plot near or along the cotectic between anorthite and tridymite, whereas most glasses plot wholly within the anorthite field, indicating somewhat higher minimum temperatures. Glass compositions not presented in Figure 6 are better represented by other systems, usually KAlSi_3O_8 - $\text{NaAlSi}_3\text{O}_8$ - SiO_2 or Al_2O_3 - KAlSi_3O_8 - SiO_2 .

For some glass compositions (e.g., 83EM5-A; DR-4A) the projection scheme described above is complicated by the presence of a fourth major normative component. Because few experimental data are available for quaternary systems approximating these glass compositions, an average minimum temperature determined from different ternary systems is presented in Table 2. One glass composition (KM-22) best represented in the system Al_2O_3 - KAlSi_3O_8 - SiO_2 plots in a liquidus field with steep isotherms, and the minimum temperature estimated for this glass is probably subject to somewhat larger systematic error. The presence of additional glass components, primarily Fe_2O_3 and P_2O_5 , may reduce these temperature estimates by ca. 20–40 °C.

If present, water, carbon dioxide, or other volatiles could shift the liquidus of paralava to somewhat lower temperatures relative to the anhydrous case. Although the effect of water on lowering the liquidus is minor at pressures near 1 bar, it should be considered, especially if ground water was involved in the burning process. At high temperatures, however, any water would probably dissociate to H_2 and form either CO or CO_2 , depending on oxygen fugacity. Furthermore, the lack of hydrous phases and a generally small loss on ignition (LOI) (Table 3) is evidence against significant H_2O in the paralavas examined. Therefore, despite the limitations in quantifying volatile concentrations, the water content is probably low, and the calculated minimum temperatures are probably reli-

able. In general, corundum-normative compositions yielded the highest minimum temperatures of formation (Table 2).

Individual residual detrital quartz grains often have a distinct melt developed along their margins, which grades into a matrix glass (Fig. 3D). Analyses indicate that the glass around the quartz is slightly enriched in silica relative to the matrix glass (GR-11A and -11B; C58-A and -B, Table 2) and most likely represents a quenched (transient) diffusion profile. XRD studies of some detrital SiO_2 grains with glass rinds reveal the presence of low-quartz, tridymite, and cristobalite. Evidently, local heating and quenching in some cases is fast enough to prevent the complete conversion of the detrital quartz to tridymite or cristobalite. High quartz melts at approximately 1423 °C, whereas cristobalite melts at a significantly higher temperature of 1723 °C (Chase et al., 1985). However, the differential substitution of even minor additional components in the SiO_2 phases may markedly affect the phase diagram (Essene, 1982). Therefore, solid solutions combined with rapidly varying temperature may lead to the metastable formation and/or persistence of one or more of the polymorphs.

Temperatures of melting determined from underground coal-gasification experiments in the Powder River Basin have been measured directly (> 1100 °C) and compared to estimates based completely on petrographic observations (Craig et al., 1983; Ethridge et al., 1983; Youngberg et al., 1983a, 1983b). These workers estimated the temperatures of melting to be in the range of 1200 to 1400 °C based on the melting points of simple phases such as cristobalite, cordierite, mullite, plagioclase, and tridymite. One caveat to this approach is that fusion temperatures for a given phase may be greatly reduced by addition of solid solutions or fluxing by a liquid. For example, the growth of cristobalite phenocrysts or the melting of cristobalite in paralavas (or lavas) by no means requires a temperature of 1723 °C (unless the liquid that forms is pure SiO_2). Therefore, the appearance or disappearance of a solid phase in multicomponent melts may lead to erroneously high estimates of temperature and should not be used for geothermometry.

WHOLE-ROCK COMPOSITIONS OF CLINKER AND PARALAVA

Samples of clinker that were examined from the Powder River Basin display variations of up to 15 wt% among its major oxides (SiO_2 , Al_2O_3 , K_2O , and CaO ; Table 3). This variation probably reflects local heterogeneity related to small changes in the original sedimentary rock. In contrast, paralava compositions are much more variable and, when compared to compositions of clinker from the same rock, display marked enrichments in Fe, Mg, and Ca and depletions in Si, Al, and K (e.g., 83EU-3A, -3B; DR4A-1, -2; Table 3). From the preliminary compositional data in Table 3 and the assumption that paralava is derived from fused clinker, it does not appear possible to generate any of the paralava compositions from whole-

TABLE 2. Glass compositions and CIPW norms of Powder River Basin paralavas

Sample:	KM-5	KM-22	GR-11A	GR-11B	83EM-5A	83EM-5B	G-11	G-7	83EU-3A
SiO ₂	83.03	71.62	69.46	72.31	71.22	76.37	75.24	74.65	75.64
TiO ₂	0.18	0.14	0.53	0.40	0.52	0.61	0.04	1.06	0.06
Al ₂ O ₃	8.38	13.47	14.64	13.58	15.53	12.35	11.70	12.81	12.78
Fe ₂ O ₃	0.44	1.18	3.77	2.51	0.81	0.50	2.77	1.58	1.21
MgO	0.04	0.41	0.98	0.74	0.06	0.13	0.16	0.14	0.06
CaO	0.38	0.30	2.92	2.56	3.64	1.05	0.17	1.14	3.23
Na ₂ O	0.22	0.16	0.17	0.21	1.86	1.45	0.35	0.36	n.d.
K ₂ O	6.00	8.52	6.78	7.27	5.09	6.27	9.76	7.80	7.22
P ₂ O ₅	0.05	0.13	0.06	0.03	0.12	0.20	0.12	0.17	0.26
F ₂	0.15	0.15	0.15	0.08	0.05	0.10	n.d.	n.d.	n.d.
F=O	0.06	0.06	0.06	0.03	0.02	0.04	n.d.	n.d.	n.d.
Total	98.81	96.02	99.40	99.66	98.88	98.99	100.31	99.71	100.46
Q	59.20	39.17	35.63	37.12	33.88	42.76	35.47	40.65	41.71
C	1.35	4.28	2.25	0.98	0.75	1.99	0.54	2.12	0.0
or	35.89	52.43	40.31	43.10	30.42	37.43	57.50	46.23	42.47
ab	1.88	1.41	1.45	1.79	15.92	12.40	2.95	3.06	0.0
an	0.53	0.36	13.13	12.00	17.17	3.34	0.06	4.56	13.49
di	0.0	0.0	0.0	0.0	0.0	0.0	0.0	0.0	0.32
en	0.10	1.06	2.45	1.85	0.15	0.32	0.40	0.35	0.0
ac	0.0	0.0	0.0	0.0	0.0	0.0	0.0	0.0	0.0
hem	0.45	1.23	3.79	2.52	0.82	0.51	2.76	1.58	1.20
ti	0.0	0.0	0.0	0.0	0.0	0.0	0.0	0.0	0.15
ap	0.12	0.31	0.14	0.07	0.28	0.46	0.28	0.39	0.60
ru	0.18	0.15	0.53	0.40	0.53	0.62	0.04	1.06	0.0
fl	0.30	0.32	0.30	0.16	0.08	0.17	0.0	0.0	0.0
T _{min} (°C)	1290	1400	1240	1230	1090	1100	1040	1080	1250

Sample:	83EU-3B	GR8-A	GR8-B	AM-13	C-58A	C-58B	DR-4A	83E-13
SiO ₂	73.58	72.04	73.49	71.83	76.25	74.97	72.62	71.28
TiO ₂	n.d.	0.76	0.53	0.14	0.27	0.22	1.02	0.35
Al ₂ O ₃	13.61	14.21	13.02	16.06	11.52	11.68	13.29	14.52
Fe ₂ O ₃	0.88	1.56	1.06	1.50	0.71	0.80	3.06	0.59
MgO	0.04	0.85	0.77	0.06	0.16	0.11	0.72	0.01
CaO	1.11	3.00	2.02	5.21	0.49	0.48	1.86	1.22
Na ₂ O	0.05	0.17	0.12	0.11	0.43	0.79	0.55	0.03
K ₂ O	10.42	7.05	7.71	5.68	9.61	9.93	8.05	12.25
P ₂ O ₅	0.11	0.32	0.23	0.79	0.11	0.18	0.05	0.22
F ₂	0.18	0.64	0.09	n.d.	0.14	0.27	0.05	0.37
F=O	0.08	0.27	0.04	n.d.	0.06	0.11	0.02	0.16
Total	99.71	99.68	98.82	100.99	99.63	99.10	101.22	100.41
Q	31.34	37.32	38.64	38.93	36.53	32.73	33.35	22.51
C	0.48	1.60	1.15	1.21	0.13	0.0	0.46	0.0
or	61.73	41.71	46.09	33.24	57.00	59.18	47.00	72.06
ab	0.42	1.44	1.03	0.92	3.65	4.83	4.59	0.25
an	4.84	12.83	9.22	23.00	0.77	0.0	8.64	3.29
di	0.0	0.0	0.0	0.0	0.0	0.0	0.0	0.0
en	0.10	2.12	1.94	0.15	0.40	0.24	1.77	0.02
ac	0.0	0.0	0.0	0.0	0.0	1.68	0.0	0.0
hem	0.88	1.56	1.07	1.49	0.71	0.22	3.02	0.59
ti	0.0	0.0	0.0	0.0	0.0	0.54	0.0	0.56
ap	0.12	0.35	0.32	0.92	0.25	0.21	0.05	0.25
ru	0.0	0.76	0.54	0.14	0.27	0.0	1.01	0.12
fl	0.09	0.30	0.0	0.0	0.28	0.27	0.10	0.35
T _{min} (°C)	1080	1240	1210	1310	1020	1030	1030	1200

Note: T_{min} = minimum temperature; n.d. = not determined.

sale melting of clinker. Although it is possible that clinker may represent a more refractory composition than paralava, evidence from both field and thin-section observations indicate that given the appropriate time, clasts of clinker melt when in contact with paralava. The most striking compositional difference between the clinkers and paralavas analyzed for this study is the concentrations of Fe. The mechanism for Fe enrichment in paralavas is not entirely understood. The Fe may come from the breakdown of detrital ferromagnesian phases in the melted sed-

imentary rocks, but chemical analyses of unfused clinker in this investigation reveal low total Fe contents (Table 3). Alternatively, Fe that was formerly in thin layers of ferruginous nodules (Table 3), or perhaps in unburned coal, may now be concentrated in the clinker after having been transferred by liquids or gases that filtered through fractures in the clinker.

Liquid immiscibility has been proposed as a mechanism for the formation of silicate and phosphatic liquids formed in combustion-metamorphic rocks associated with

TABLE 3. Whole-rock compositions and CIPW norms of Powder River Basin clinker and paralava

Sample: Rock type:	83EU-3A Clinker	83EU-3B Paralava	KM-4 Clinker	DR-9 Clinker	DR4A-1 Clinker	DR4A-2 Paralava	DR2 Fe nodule
SiO ₂	74.31	48.95	63.67	68.88	66.98	50.04	22.90
TiO ₂	0.83	0.60	0.52	0.74	0.86	0.71	0.23
Al ₂ O ₃	16.39	11.31	10.05	16.25	21.85	21.77	5.13
Fe ₂ O ₃	3.62	38.08	2.64	4.18	3.20	6.94	42.79
MnO	0.02	0.26	0.06	0.04	0.01	0.13	0.93
MgO	0.79	1.30	5.09	2.89	1.45	2.61	2.59
CaO	0.16	1.14	15.05	2.97	0.92	14.00	18.19
Na ₂ O	0.34	0.01	0.13	0.48	0.25	n.d.	0.09
K ₂ O	2.29	1.61	2.25	2.65	2.69	1.35	0.44
P ₂ O ₅	0.04	0.26	0.29	0.16	0.05	0.44	8.09
H ₂ O*	0.21	0.96	0.02	0.10	0.16	0.72	0.22
LOI*	0.21	-1.42	0.06	0.09	-1.07	0.24	0.11
Total	98.79	103.52	99.75	99.24	98.26	97.98	101.41
Q	63.15	39.19	26.78	46.28	53.32	15.04	6.28
C	13.37	8.12	0.0	7.67	17.33	0.0	0.0
or	13.75	9.54	13.37	15.85	16.23	8.20	2.68
ab	2.93	0.08	1.11	4.11	2.16	0.0	0.78
an	0.54	3.97	20.29	13.85	4.33	56.96	12.66
di	0.0	0.0	27.48	0.0	0.0	7.36	14.33
en	2.00	3.25	0.0	7.29	3.69	3.27	0.0
wo	0.0	0.0	6.66	0.0	0.0	0.0	3.11
mt	0.0	0.0	0.0	0.0	0.0	0.0	2.44
il	0.04	0.56	0.13	0.09	0.02	0.29	0.45
hem	3.68	38.19	2.65	4.23	3.27	7.13	42.39
ti	0.0	0.0	1.12	0.0	0.0	1.42	0.0
ap	0.09	0.60	0.67	0.37	0.12	1.05	19.30
ru	0.82	0.31	0.0	0.70	0.87	0.0	0.0

Note: n.d. = not determined.

* Includes H₂O, CO₂, SO₂.

bituminous sedimentary rocks (Bentor et al., 1981). The Fe enrichments observed in paralava, when compared to clinker, may also be explained by liquid immiscibility. Comparison of experimental and natural occurrences of basalt formed at high temperature and conditions of high f_{O_2} indicate a field of liquid immiscibility that becomes larger with increased f_{O_2} (Naslund, 1983). The position of this immiscibility field is outlined in Figure 7 together with the position of whole-rock and glass compositional data from paralava. Paralava and glass compositions are strikingly similar to natural and experimental immiscible liquids, a fact which suggests that liquid immiscibility may be a viable mechanism for generating some paralava compositions. If the Fe-rich paralava, which often forms flows and injections, represents an immiscible silicate liquid, then an Fe-depleted residue should remain elsewhere. One possible candidate for this residue is the paralava at the coal-sedimentary rock interface; however, further work is necessary to test this hypothesis. In most geologic environments where immiscible liquids have been observed, the immiscible phases are not greatly separated. However, if liquid immiscibility is an effective mechanism for generating the compositional variation observed in paralavas, then a more efficient liquid separation phenomenon may be indicated.

OXIDATION-REDUCTION RELATIONS

Oxidation (burning) of coal can readily reduce clinker in a natural fashion that is analogous to the Fe-smelting process. Indeed, small amounts of native iron have been

reported in clinkers from Edmonton, Canada (Tyrrell, 1887) and South Australia (Baker, 1953). In the Powder River Basin, clinkers and paralavas are less reduced, with many samples containing hematite, magnetite, and/or fayalite. Paralava and clinker containing magnetite and/or hematite acquire a high-intensity thermoremanent magnetization that appears to faithfully record the ambient geomagnetic field, allowing mapping of burn zones (Jones et al., 1982) and tracing of magnetic reversals in ancient burns (Jones et al., 1984; Cisowski and Fuller, 1987). The demagnetization experiments of Jones et al. (1984) indicate that remanent magnetization is contained in titanomagnetite, hematite, and goethite, but that the predominant magnetization in clinker resides in titanomagnetite. The highest magnetic susceptibilities in clinker may develop from those sedimentary rocks that are least permeable to oxygen (Hooper, 1984).

Mineral assemblages and compositions of paralavas may be influenced partly by the composition and partial pressure of gas produced during coal combustion. As the gases are produced from burning coal, they may continually mix with any additional fluids and/or gases present. Mixing of this sort may produce significant variation in the composition of these gases, which may be calculated by combining thermochemical data with chemical reactions in the system C-O-H. It is difficult to evaluate the role of H-bearing gas species in these calculations because of a lack of hydrous phases in paralavas. Although interaction with ground water could conceivably introduce significant H₂O that may react to form H₂ and/or CH₄

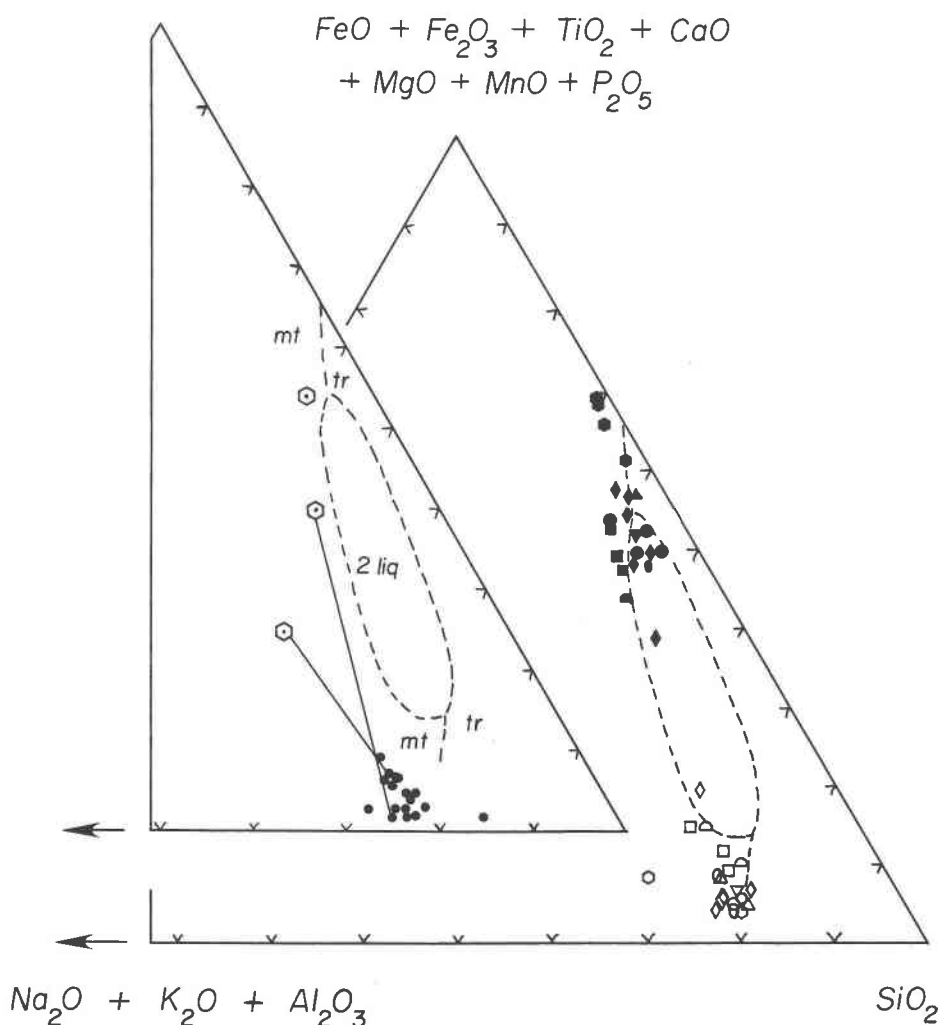


Fig. 7. Field of liquid immiscibility for basalts determined experimentally under oxidizing conditions ($\log_{10} f_{O_2} = 10^{-9}$) (Naslund, 1983); mt = magnetite; tr = tridymite; 2 liq = two liquids. Paralava glasses (filled dots) and some coexisting paralava (hexagons) are shown in the left projection. Positions of experimental and natural coexisting immiscible liquids in basalts are shown on the right projection (data taken from Kuo et al., 1986).

under more reducing conditions during coal combustion, we will assume a system dominated by C and O. Ultimately, direct gas sampling at active burning areas or measurement of fluid inclusions in the paralava phenocrysts may lead to a better understanding of the gas composition.

Examination of several paralava samples from a single outcrop reveals marked contrasts in mineral content that may reflect different oxidation states. For example, paralava within the coal-ash layer described earlier may contain the phases pyroxene, melilite, anorthite, magnetite-ulvöspinel-hercynite solid solutions and glass, whereas paralava occurring in chimneys above the coal-ash zone often contain fayalite, tridymite, abundant magnetite-ulvöspinel-hercynite solid solutions, cordierite, late hematite, and lesser glass. The contrasting mineral content requires steep gradients in f_{O_2} . Assuming that the coal-

sedimentary rock interface is in equilibrium with graphite (i.e., $a_C = 1$), using tabulated ΔG^0 data for CO and CO₂ (Robinson et al., 1982) the position of graphite stability in T - f_{O_2} space may be calculated by solving the following simultaneous reactions:

$$2C + O_2 = 2CO \quad (1)$$

and

$$C + O_2 = CO_2 \quad (2)$$

and

$$P_{tot} = P_{CO} + P_{CO_2} \quad (3)$$

Figure 8 illustrates the position of this curve at surface pressures. A paralava bearing the quartz + fayalite + magnetite (QFM) assemblage was collected from one to several meters above the coal-sedimentary rock inter-

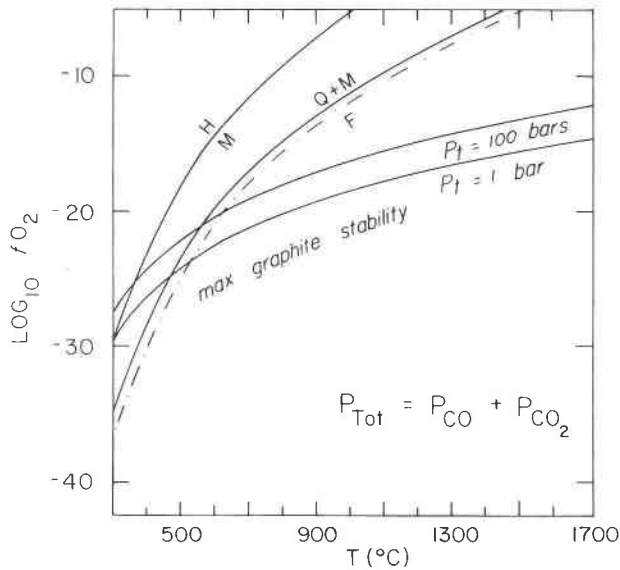


Fig. 8. T - f_{O_2} plot of the following reactions: 4 Magnetite + $O_2 = 6$ Hematite (HM); 3 Fayalite + $O_2 = 2$ Magnetite + 3 Quartz (QFM); $C + O_2 = CO_2$; and $2C + O_2 = 2CO$, for conditions of $P_{tot} = P_{CO} + P_{CO_2}$ and $a_c = 1$. Dot-dash line accounts for reduced activity in the solid phases assuming ideal mixing.

face; this paralava places additional constraints on f_{O_2} . Using tabulated free energies for fayalite (Fa), quartz, and magnetite (Mt) (Robinson et al., 1982) and correcting for solid solutions, the values of f_{O_2} at a given temperature for this reaction may be calculated by solving the following equation:

$$\Delta G_T = \Delta G_T^0 + RT \ln(f_{O_2})(X_{Fa}^{O_2})^3 - RT \ln(X_{Mt}^{O_2})^2. \quad (4)$$

Figure 8 contains the position of this curve for the QFM-bearing paralava relative to pure QFM and relative to paralava in equilibrium with C. The gradients in f_{O_2} between these paralavas therefore require variations of several logs units at high temperature. The composition of the gas phase associated with either of the above paralavas, calculated with the assumptions $P_{fluid} = P_{CO} + P_{CO_2} = P_{tot} = 1$ bar, is represented in Figure 9. Paralava in equilibrium with graphite (i.e., at the coal-sedimentary rock interface at 1 bar) has CO as the dominant gas species at temperatures above about 650 °C. Below that temperature, CO_2 is dominant. Pressure increases of several hundred bars have little effect on these results.

Because the coal-ash paralavas indicate oxidation states approaching those of the hematite-magnetite buffer (Cosca and Peacor, 1987), they did not remain in equilibrium with C. Remnant coal is often present, however, indicating gradients of at least five orders of magnitude in f_{O_2} (and a_c) over a few centimeters to meters of the burning coal bed.

No vertical gradients in f_{O_2} were detected from chemical analyses of the oxide phases at different elevations in a chimney structure. Oxides at various levels of the chimney consist of solid solutions of magnetite-hercynite-ul-

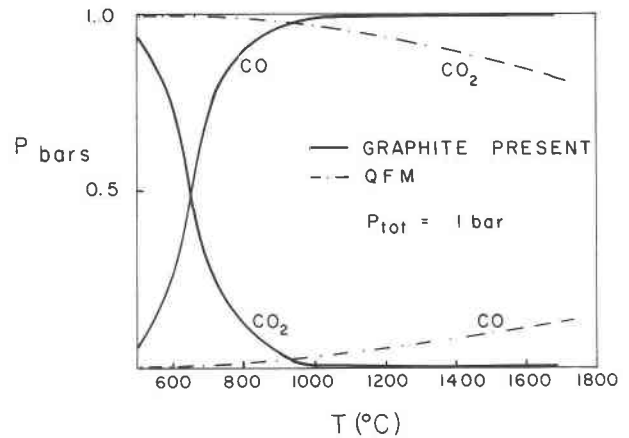


Fig. 9. Plot of partial pressures of CO and CO_2 in the system C-O calculated for a total pressure of 1 bar and for conditions of either graphite or QFM present.

vöspinel often with hematite-ilmenite and pseudobrookite lamellae. The complex exsolution and oxidation patterns in the oxides may in part be due to changes in f_{O_2} with time. This interpretation is suggested by hematite overgrowths on or exsolutions from many of the magnetite solid solutions. Late hematite is also observed concentrated around vesicles, but it appears unrelated to vertical position in the chimney (Fig. 4F). Factors locally affecting progressive oxidation may be locally quite variable, but presumably ground water, rock porosity, fracture densities, and fluids released from clay minerals could all be important.

DISCUSSION

When interpreting the chemical variations observed in paralava, it is difficult to evaluate the exact degree to which melting or crystallization processes (or other processes) have been involved. However, certain field and petrographic observations combined with analytical data may help constrain their relative importance. For example, partial melting is certainly a mechanism at least partly responsible for the local melts formed within fractured clinker, although formation of other paralava, including that found in chimney structures or slaglike blocks, probably involved large-scale melting. Because the paralava-forming liquids reached extremely high temperatures, mechanisms such as fractional melting and/or incongruent volatilization, vapor transport, liquid mixing, or liquid immiscibility may have significantly altered the original liquidus compositions. Such processes may explain the unusual enrichments of Fe in paralava or how certain paralava compositions are driven toward silica undersaturation. Alternatively, field evidence from chimneys and flow structures indicates transportation of liquid (\pm phenocrysts) that may have digested foreign sediment (clinker) enroute, or mixed with separate fluid(s) (Cosca et al., 1988). Other possibilities like fractional crystallization and its effects on liquid composition may be im-

portant especially when interpreting phenocryst-bearing samples. Crystallization of high-temperature, refractory phases such as spinel, melilite, or mullite could substantially alter any residual glass composition relative to the original liquidus composition. Whether one process dominates another is currently difficult to evaluate, but may be better understood with a detailed evaluation of many glass and bulk-rock analyses. It is clear, however, that clinker and paralava have distinct compositional characteristics and involve some type of differential elemental remobilization.

ACKNOWLEDGMENTS

We wish to acknowledge the Kerr McGee Co. for allowing access to the Jacobs Ranch and Clovis Point Mines, and the Nerco Mining Co. for access to the Antelope Coal Mine. B. H. Wilkinson is thanked for drawing our attention to combustion metamorphic outcrops in Utah. Kudos to C. E. Henderson for maintaining the electron microprobe in excellent working condition and to R. J. Arculus for helpful discussions and for instruction with xrf analyses. Discussions with A. Afifi, A. T. Anderson, and S. R. Bohlen and comments by R. B. Finkelman, W. J. Harrison, P. J. Modreski, W. P. Nash, and an anonymous reviewer are gratefully acknowledged. This study was supported by grants from the Geological Society of America, Sigma Xi, and the Turner Fund of the University of Michigan to M.A.C. Some aspects of this research were additionally supported by NSF grant EAR-84-08169 to E.J.E. The electron-microprobe analyzer used in this work was acquired under Grant EAR-82-12764 from the NSF.

REFERENCES CITED

- Agrell, S.O., and Langley, J.M. (1958) The dolerite plug at Tierebullaigh, near Cushendall, County Antrim, Proceedings of the Royal Irish Academy, 59, 92–128.
- Baker, G. (1953) Naturally fused coal ash from Leigh Creek, South Australia. Transactions of the Royal Society of Southern Australia, 76, 1–20.
- Bastin, E.S. (1905) Note on baked clays and natural slags in eastern Wyoming. Journal of Geology, 13, 408–412.
- Bauer, L.P. (1972) The alteration of sedimentary rocks due to burning coal in the Powder River Basin, Campbell County, Wyoming. M.S. thesis, Texas Tech University, Lubbock, Texas.
- Bentor, Y.K. (1984) Combustion-metamorphic glasses. Journal of Non-Crystalline Solids, 67, 443–448.
- Bentor, Y.K., and Kastner, M. (1976) Combustion metamorphism in southern California. Science, 193, 486–488.
- Bentor, Y.K., Kastner, M., Perlman, I., and Yellin, Y. (1981) Combustion metamorphism of bituminous sediments and the formation of melts of granitic and sedimentary composition. Geochimica et Cosmochimica Acta, 45, 2229–2255.
- Brady, L.F., and Greig, J.W. (1939) Note on the temperature attained in a burning coal seam. American Journal of Science, 237, 116–119.
- Budai, C.M., and Cummings, M.L. (1984) Geologic controls of coal burns and oxidized zones in the Antelope Coal Field, Converse County, Wyoming. In R.L. Houghton, Ed., Symposium on the geology of Rocky Mountain coal, 84-1, p. 168–183. Geological Society of North Dakota, Bismarck, North Dakota.
- Bustin, R.M., and Mathews, W.H. (1982) In situ gasification of coal, a natural example: History, petrology, and mechanics of combustion. Canadian Journal of Earth Sciences, 19, 514–523.
- Chase, M.W., Jr., Davies, C.A., Downey, J.R., Jr., Frurip, D.J., McDonald, R.A., and Syverud, A.N. (1985) JANAF thermochemical tables (third edition). In D.R. Lide, Ed., Journal of Physical and Chemical Reference Data, 14, 1856 p.
- Church, B.N., Matheson, A., and Hora, Z.D. (1979) Combustion metamorphism in the Hat Creek area, British Columbia. Canadian Journal of Earth Sciences, 16, 1882–1887.
- Cisowski, S.M., and Fuller, M. (1987) The generation of magnetic anomalies by combustion metamorphism of sedimentary rock, and its significance to hydrocarbon exploration. Geological Society of America Bulletin, 99, 21–29.
- Clark, B.H., and Peacor, D.R. (1987) Mineralogic and textural transitions in shales due to pyrometamorphism and incipient melting (abs.). EOS, 68, 452.
- Coates, D.A., and Naeser, C.W. (1984) Map showing fission-track ages of clinker in the Rochelle Hills, southern Campbell County Wyoming. U.S. Geological Survey Miscellaneous Investigations Series Map I-1462.
- Cosca, M.A., and Essene, E.J. (1985) Paralava chemistry and conditions of formation, Powder River Basin, Wyoming (abs.). EOS, 66, 396.
- Cosca, M.A., and Peacor, D.R. (1987) Chemistry and structure of eseneite, CaFeAlSiO_6 , a new pyroxene produced by pyrometamorphism. American Mineralogist, 72, 148–156.
- Cosca, M.A., Peacor, D.R., and Essene, E.J. (1985) The chemistry and structure of a natural ferri-aluminum tschermakitic pyroxene produced by pyrometamorphism. Geological Society of America Abstracts with Programs, 17, 553.
- Cosca, M.A., Rouse, R.C., and Essene, E.J. (1988) Dorrite $\text{Ca}_2(\text{Mg}, \text{Fe}^{2+})\text{-(Al}_2\text{Si}_2\text{O}_{20})$, a new member of the aenigmatite group from a pyrometamorphic melt-rock. American Mineralogist, 73, 1440–1448.
- Craig, G.N., Burns, L.K., Ethridge, F.G., Laughter, T.F., and Youngberg, A.D. (1983) Overburden characterization and post-burn study of the Hoe Creek, Wyoming Underground Coal Gasification site and comparison with the Hanna, Wyoming site. U.S. Department of Energy Publication DOE/LC/10496-T1, 188 p.
- Denson, N.M., and Keefer, W.R. (1974) Map of the Wyodak-Anderson coal bed in the Gillette area, Campbell County, Wyoming. U.S. Geological Survey Miscellaneous Investigations Series Map I-848-D, scale 1:125000.
- Essene, E.J. (1982) Geologic thermometry and barometry. Mineralogical Society of America Reviews in Mineralogy, 10, 153–206.
- Essene, E.J., Coates, D.A., Geissman, J.W., and Simmons, W.B. (1984) Paralavas formed by burning of coal beds (abs.). EOS, 65, 300.
- Ethridge, F.G., Burns, L.K., Alexander, W.G., Craig, G.N., and Youngberg, A.D. (1983) Overburden characterization and post-burn study of the Hoe Creek, Wyoming Underground Coal Gasification site and comparison with the Hanna, Wyoming site. U.S. Department of Energy Publication DOE/LC/10705-T1, 185 p.
- Fermor, L.L. (1918) Preliminary note on the burning of coal seams at the outcrop. Transactions of the Mining, Geological, and Metallurgical Institute of India, 12, 50–63.
- Foit, F.F., Jr., Hooper, R.L., and Rosenberg, P.E. (1987) An unusual pyroxene, melilite, and iron oxide mineral assemblage in a coal-fire buchite from Buffalo, Wyoming. American Mineralogist, 72, 137–147.
- Glass, G.B. (1976) Update on the Powder River coal basin. In R.B. Laudon, Ed., Geology and energy resources of the Powder River Basin, 28th Annual Field Conference Guidebook, p. 209–220. Wyoming Geological Association, Casper, Wyoming.
- Gleason, J.D., and Kyser, T.K. (1984) Stable isotope compositions of gases and vegetation near naturally burning coal. Nature, 307, 254–257.
- Grapes, R.H. (1986) Melting and thermal reconstitution of pelitic xenoliths, Wehr Volcano, East Eifel, West Germany. Journal of Petrology, 27, 343–396.
- Hooper, R.L. (1982) Mineralogy of a coal burn near Kemmerer, Wyoming. M.S. thesis, Washington State University, Pullman, Washington.
- (1984) Factors affecting the magnetic susceptibility of baked rocks above a burned coal seam. Geological Society of America Abstracts with Programs, 16, 543.
- Hooper, R.L., and Foit, F.F. (1986) Pyroxenes and melilites with extensive tetrahedral Fe^{3+} substitution from a coal-fire buchite near Buffalo, Wyoming (abs.). EOS, 67, 1270.
- Jackson, K.C. (1981) Clinker genesis and the comparison of naturally occurring clinker to compounds in the system $\text{FeO-Al}_2\text{O}_3\text{-SiO}_2$. B.S. thesis, Beloit College, Beloit, Wisconsin.
- Jones, A.H., Geissman, J.W., Coates, D.A., Naeser, C.W., and Heffern, E.L. (1982) Paleomagnetism of Powder River Basin clinker, Wyoming and Montana: Documentation of Bruhnes and Matuyama burning of Tertiary coals (abs.). EOS, 63, 304.
- Jones, A.H., Geissman, J.W., and Coates, D.A. (1984) Clinker deposits,

- Powder River Basin, Wyoming and Montana: A new source of high-fidelity paleomagnetic data for the Quaternary. *Geophysical Research Letters*, 11, 1231-1234.
- Kuo, L.-C., Lee, J.H., Essene, E.J., and Peacor, D.R. (1986) Occurrence, chemistry, and origin of immiscible silicate glasses in a tholeiitic basalt: A TEM/AEM study. *Contributions to Mineralogy and Petrology*, 94, 90-98.
- Lofgren, G., Donaldson, C.H., Williams, R.J., Mullins, O., Jr., and Usselman, T. (1974) Experimentally reproduced textures and mineral chemistry of Apollo 15 quartz normative basalt. In W.A. Gose, Ed., *Proceedings of the 5th Lunar and Planetary Science Conference*, 1, 549-569. Pergamon, New York.
- Matthews, A., and Gross, S. (1980) Petrologic evolution of the "Mottled Zone" (Hatrumim) metamorphic complex of Israel. *Israel Journal of Earth Science*, 29, 93-106.
- May, P.R. (1954) Clinker. In *North Dakota Geological Society Guidebook, Southwestern North Dakota Field Conference*, 18-19.
- McLintock, W.F.P. (1932) On the metamorphism produced by the combustion of hydrocarbons in the Tertiary sediments of south-west Persia. *Mineralogical Magazine*, 23, 207-227.
- Merritt, R.D. (1985) Review of coking phenomena in relation to an occurrence of prismatically fractured natural coke from the Castle Mountain Mine, Matanuska coal field, Alaska. *International Journal of Coal Geology*, 4, 281-298.
- Modreski, P.J., and Herring, J.R. (1985) High-temperature hematite and spinel phases in iron-rich slags produced in shales above burned coal beds. *Geological Society of America Abstracts with Programs*, 17, 666.
- Naslund, H.R. (1983) The effect of oxygen fugacity on liquid immiscibility in iron-bearing silicate melts. *American Journal of Science*, 283, 1034-1059.
- Osborn, E.F., and Muan, A. (1960) *Phase equilibrium diagrams of oxide systems*. The American Ceramic Society, Columbus, Ohio.
- Phemister, J. (1942) Note on fused spent shale from a retort at Pumpherton, Midlothian. *Transactions of the Geological Society of Glasgow*, 20, 238-246.
- Raask, E. (1985) *Mineral impurities in coal combustion: Behavior, problems, and remedial measures*, 484 p. Hemisphere Publishing, Washington, D.C.
- Robinson, G.R., Jr., Haas, J.L., Jr., Schafer, C.M., and Haselton, H.T., Jr. (1982) Thermodynamic and thermophysical properties of selected phases in the MgO-SiO₂-H₂O-CO₂, CaO-Al₂O₃-SiO₂-H₂O-CO₂, and FeO-Fe₂O₃-SiO₂ chemical systems with special emphasis on the properties of basalts and their mineral component. U.S. Geological Survey Open-File Report 83-79, 429 p.
- Rogers, G.S. (1918) Baked shale and slag formed by the burning of coal beds. U.S. Geological Survey Professional Paper 108-A, 1-10.
- Schairer, J.F. (1950) The alkali-feldspar join in the system NaAlSi₃O₈-KAlSi₃O₈-SiO₂. *Journal of Geology*, 58, 512-517.
- Schairer, J.F., and Bowen, N.L. (1947) The system leucite-anorthite-silica. *Geological Society of Finland Bulletin*, 20, 67-87.
- Schneider, H., and Majdic, A. (1984) Iron incorporation in tridymite and cristobalite. *Neues Jahrbuch für Mineralogie Monatshefte*, 559-568.
- (1985) Titanium incorporation in tridymite. *Neues Jahrbuch für Mineralogie Monatshefte*, 418-426.
- Seifert-Kraus, U., and Schneider, H. (1984) Cation distribution between cristobalite, tridymite, and coexisting glass phase in used silica bricks. *Ceramics International*, 10, 135-142.
- Sigsby, R.J. (1966) "Scoria" of North Dakota. Ph.D. thesis, University of North Dakota, Grand Forks, North Dakota.
- Smith, D.G.W. (1969) Pyrometamorphism of phyllites by a dolerite plug. *Journal of Petrology*, 10, 20-55.
- Tilley, C.E. (1924) Contact metamorphism in the Comrie area of the Perthshire Highland. *Quarterly Journal of the Geological Society of London*, 80, 22-71.
- Tyrell, J.B. (1887) Naturally reduced iron. *American Journal of Science*, 33, 73.
- Venkatesh, V. (1952) Development and growth of cordierite in para-lava. *American Mineralogist*, 37, 831-848.
- West, W.E. (1964) The Powder River Basin. In E.R. Keller and R.E. Glaze, Eds., *Highway geology of Wyoming*, p. 20-28. Wyoming Geological Association, Casper, Wyoming.
- Whitworth, H.F. (1958) The occurrence of some fused sedimentary rocks at Ravensworth, N.S.W. *Journal of the Royal Society of New South Wales*, 92, 204-210.
- Wyllie, P.J. (1961) Fusion of a Torridonian sandstone by a picrite sill in Soay (Hebrides). *Journal of Petrology*, 2, 1-37.
- Youngberg, A.D., McClurg, J.E., and Schmitt, J.G. (1983a) Depositional environments, subsurface stratigraphy, and post-burn characterization of the Paleocene-Eocene Hanna, Wyoming Underground Coal Gasification Site. Hanna III experiment. U.S. Department of Energy Publication DOE/LC/RT-83-1, 120 p.
- (1983b) Depositional environments, subsurface stratigraphy, and post-burn characterization of the Paleocene-Eocene Hanna Formation at the Hanna, Wyoming Underground Coal Gasification Site. Hanna II phase I experiment. U.S. Department of Energy Publication DOE/LC/R1-83-2, 163 p.

MANUSCRIPT RECEIVED APRIL 25, 1988

MANUSCRIPT ACCEPTED SEPTEMBER 27, 1988